Progress In Electromagnetics Research, Vol. 158, 7–20, 2017

High Order Extractions of Broadband Green's Function with Low Wavenumber Extractions for Arbitrary Shaped Waveguide

Tien-Hao Liao[1, *], Kung-Hau Ding[2], and Leung Tsang[1]

Abstract—In this paper we develop a higher order extraction method to accelerate the convergence in the computation of broadband Green's function (BBGFL) for an arbitrary shaped homogeneous waveguide.The broadband Green's function is based on modal expansions in which the modal field solutions are frequency independent. The higher order extraction is obtained by using three low wavenumbers in extraction. It gives a modal expansion of Broadband Green's Function with 6th order convergence requiring fewer evanescent modes for convergence. Numerical results are illustrated for both lossless and lossy dielectric cases. The accuracy of results are verified with direct method of moment (MoM) and HFSS. The higher order BBGFL method is computationally efficient for broadband simulations.

1. INTRODUCTION

Green's functions are important in electromagnetic theory as they are the responses of the electromagnetic fields of point sources that give physical understandings of the problems. They are also useful for formulating integral equations for boundary values problems [1–4]. Commonly used Green's functions include free space Green's functions, periodic Green's functions for empty periodic lattices, and Green's functions of regular geometry such as a sphere or cylinder, Green's functions of layered media, etc. However, these are Green's functions at a single frequency and are for regular geometries. Recently, the Green's function technique has been used to study the problems of signal integrity (SI) and electromagnetic compatibility (EMC) in printed circuit boards (PCBs), including the effects of vias for infinite ground plane and for finite ground plane [5–7]. In the past studies, the free space Green's functions were used. The disadvantage of using the free space Green's function is that, one has to solve the boundary value problem of an arbitrary shaped waveguide for each frequency. For broadband simulations using integral equations, the dense matrix equation of MoM needs to be solved for each frequency. In this paper, we develop broadband Green's functions for arbitrary shaped waveguides using a higher order extraction method to achieve accelerated convergence in computing responses.

The Boundary Integral-Resonant Mode Expansion (BIRME) method was invented to calculate the modes of an arbitrary shaped waveguide [8–10]. The BIRME method uses the DC extraction of rectangular and circular waveguides to calculate the modes of an arbitrary shaped homogeneous waveguide [8–10]. Recently, we have developed the method of broadband Green's function with low wavenumber extraction (BBGFL) to calculate the BBGFL of homogenous waveguide of arbitrary shape [11, 13–16]. The BBGFL is a method of calculation and is also a quantity to be calculated. We begin with the BBGFL of rectangular waveguide and use the method of BBGFL to calculate the BBGFL

Received 10 October 2016, Accepted 6 December 2016, Scheduled 31 December 2016

* Corresponding author: Tien-Hao Liao (tienliao@umich.edu).

[1] Radiation Laboratory, Department of Electrical Engineering and Computer Science, The University of Michigan, Ann Arbor, MI 48109-2122, USA. [2] Antenna and Electromagnetics Technology Branch, Sensors Directorate, Air Force Research Laboratory, Wright-Patterson AFB, USA.

of arbitrary shaped waveguide [11]. Unlike BIRME, the BBGFL uses a low wavenumber extraction. The MoM is applied in BBGFL a single time for low wavenumber extraction. We then compute the modes of an arbitrary shaped waveguide using the BBGFL of rectangular waveguide. Then we use the modes to construct the broadband Green's function for the arbitrary shaped waveguide. The low wavenumber extraction is also applied to the arbitrary shaped waveguide. The BBGFL was combined with Foldy-Lax multiple scattering equations for the simulations of fields in arbitrarily shaped PCB power/ground planes with vias [11–13]. It was also used to study EMC problems [14]. We also applied the BBGFL method to periodic photonic structures and metamaterials [15, 16].

Previously, in the BBGFL method [11, 13–16], a single low wavenumber Green's function is extracted with the result of 4th order convergence in modal summations. The number of required evanescent modes in modal expansion are reduced.The evanescent modes are modes with modal wavenumber higher than the operating wavenumber. Using low wavenumber extraction to reduce the number of required evanescent modes is physically equivalent to the conversion of evanescent modes to near fields. In this paper we develop a higher order extraction technique. We use three low wavenumber extractions giving a 6th order convergence of modal expansion. Results show that the number of required evanescent modes are reduced significantly compared with single low wavenumber extraction. Higher order convergences are also useful when spatial first and second order derivatives of the BBGFL are often required in formulating integral equations with BBGFL. The accuracy of the BBGFL results are validated by comparing with the results of direct MoM and HFSS.

The outline of the paper is as follows. In Section 2, we derive the higher order extraction of broadband Green's function. In Section 3, we illustrate the numerical results of BBGFL for resonant modes and make comparisons of Green's function with that of direct MoM and HFSS. The computation efficiencies and error comparisons are also shown. In Section 4 we give conclusions.

2. BROADBAND GREEN'S FUNCTION WITH LOW WAVENUMBER EXTRACTION (BBGFL)

In this section we illustrate the construction of BBGFL for an irregularly shaped waveguide with cross section S and PEC boundary ∂S as shown in Figure 1(a). The homogenous waveguide is filled with dielectric with relative permittivity ε_r. There are two stages in the construction of broadband Green's function [14]. In the first stage, the BBGFL of the rectangular waveguide is applied to form the linear eigenvalue problem of modes for the irregularly shaped waveguide. A linear eigenvalue problem means that resonant modes are calculated simultaneously. Normalization of the modes are carried out. In the second stage, the broadband Green's function for the arbitrary shaped waveguide is constructed by expansion in therms of the normalized resonant modes. Next, the three low wavenumber extractions is applied to accelerate the convergence of modal summation which results in 6th order of convergence. The Green's functions at the 3 low wavenumbers are calculated using MoM.

2.1. Resonant Modes of Arbitrary Shaped Waveguide S

We consider the TM modes of waveguide S with PEC boundary ∂S as shown in Figure 1(c). The part of boundary $\partial S - \sigma$ coincides with the rectangular boundary $\partial\Omega$ of Figure 1(b). The dimensions of rectangular waveguide are L_x and L_y, and the boundary σ is (Figure 1(c)) with the dimensions of W_x and W_y. We shall denote the arbitrary shaped waveguide as waveguide S.

The modal expansion of rectangular waveguide Green's function g_E^Ω is expressed as [8]

$$g_E^\Omega\left(k,\bar{\rho},\bar{\rho}'\right)=\sum_\alpha \frac{\psi_\alpha^\Omega\left(\bar{\rho}\right)\psi_\alpha^\Omega\left(\bar{\rho}'\right)}{\left(k_\alpha^\Omega\right)^2-k^2} \tag{1}$$

where the modal functions $\psi_\alpha^\Omega(\bar{\rho})$ are given by

$$\psi_\alpha^\Omega\left(\bar{\rho}\right)=\psi_{pq}^\Omega\left(x,y\right)=\frac{2}{\sqrt{L_xL_y}}\sin\left(\frac{p\pi}{L_x}\left(x+\frac{L_x}{2}\right)\right)\sin\left(\frac{q\pi}{L_y}\left(y+\frac{L_y}{2}\right)\right) \tag{2}$$

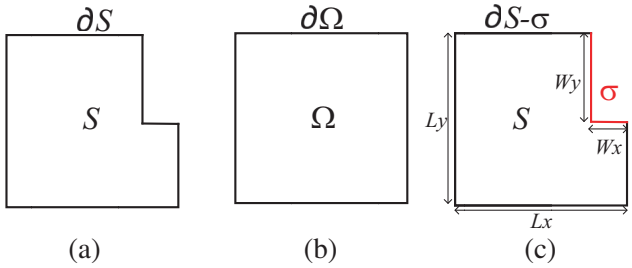

Figure 1. Waveguide with homogeneous dielectric. (a) Arbitrary shaped waveguide S with boundary ∂S. (b) Rectangular waveguide Ω with boundary $\partial\Omega$. (c) Arbitrary shaped waveguide S with boundary σ and boundary $\partial S - \sigma$ coinciding with rectangular boundary $\partial\Omega$. The dimensions of rectangular waveguide are L_x and L_y and the dimensions of boundary σ are W_x and W_y.

with p, $q = 1, 2, \ldots$, $\frac{-L_x}{2} \leq x \leq \frac{L_x}{2}$ and $\frac{-L_y}{2} \leq y \leq \frac{L_y}{2}$. The resonant wavenumbers k_α^Ω are

$$k_\alpha^\Omega = \sqrt{\left(\frac{p\pi}{L_x}\right)^2 + \left(\frac{q\pi}{L_y}\right)^2} \tag{3}$$

The modal function $\psi_\alpha^\Omega(\bar{\rho})$ satisfies the boundary condition $\psi_\alpha^\Omega(\bar{\rho}) = 0$ for $\bar{\rho}$ on $\partial\Omega$. The subscript α is the modal index for the domain Ω. It is used for the combined index pair (p, q). The subscript E in g_E^Ω denotes that the physical quantity considered is the electric field for the TM modes.

The modal summation in Eq. (1) converges slowly particularly when $\bar{\rho}$ is close to $\bar{\rho}'$. We previously used a single low wavenumber extraction to accelerate the convergence [11–14].

$$g_E^\Omega\left(k, \bar{\rho}, \bar{\rho}'\right) = g_E^\Omega\left(k_L^\Omega, \bar{\rho}, \bar{\rho}'\right) + \sum_\alpha \frac{\left[k^2 - \left(k_L^\Omega\right)^2\right] \psi_\alpha^\Omega(\bar{\rho})\, \psi_\alpha^\Omega(\bar{\rho}')}{\left[\left(k_\alpha^\Omega\right)^2 - k^2\right]\left[\left(k_\alpha^\Omega\right)^2 - \left(k_L^\Omega\right)^2\right]} \tag{4}$$

The low wavenumber ($k_L^\Omega \ll k$) term $g_E^\Omega(k_L^\Omega, \bar{\rho}, \bar{\rho}')$ is calculated readily using MoM with relatively few unknowns because the low wavenumber corresponds to low frequency solution.

Similarly, the Green's function of irregularly shaped waveguide S is expressed as

$$g_E^S\left(k, \bar{\rho}, \bar{\rho}'\right) = \sum_\beta \frac{\psi_\beta^S(\bar{\rho})\, \psi_\beta^S(\bar{\rho}')}{\left(k_\beta^S\right)^2 - k^2} \tag{5}$$

where β stands for the modal index for S and k_β^S the corresponding resonant wavenumber. The modal functions of S obeys the wave equation

$$\nabla_t^2 \psi_\beta^S(\bar{\rho}) + \left(k_\beta^S\right)^2 \psi_\beta^S(\bar{\rho}) = 0 \quad \text{for } \bar{\rho} \text{ inside } S \tag{6}$$

and the boundary condition

$$\psi_\beta^S(\bar{\rho}) = 0 \quad \text{for } \bar{\rho} \text{ on } \partial S \tag{7}$$

The subscript t stands for transverse since we are considering a 2D problem for PCB with small thickness so that only the TM0 mode propagates.

To calculate k_β^S and $\psi_\beta^S(\bar{\rho})$, we apply the Green's theorem using $\psi_\beta^S(\bar{\rho})$ and $g_E^\Omega(k, \bar{\rho}, \bar{\rho}')$. Because of the overlapping between ∂S and $\partial\Omega$ boundaries, the surface integral equation (SIE) is only over the part σ of the boundary.

$$\int_\sigma g_E^\Omega\left(k, \bar{\rho}, \bar{\rho}'\right) \hat{n}_{out}' \cdot \bar{\nabla}_t' \psi_\beta^S(\bar{\rho}')\, dl' = \begin{cases} \psi_\beta^S(\bar{\rho}) & \text{for } \bar{\rho} \text{ inside } S \\ 0 & \text{for } \bar{\rho} \text{ outside } S \end{cases} \tag{8}$$

where the unit normal vector $\hat{n}_{out}^{'}$ points outward of ∂S. Using Equation (8) and the extracted modal summation (4) of $g_E^{\Omega}(k,\bar{\rho},\bar{\rho}^{'})$ yields

$$\int_{\sigma} g_E^{\Omega}\left(k_L^{\Omega},\bar{\rho},\bar{\rho}^{'}\right)\hat{n}_{out}^{'}\cdot\bar{\nabla}_t^{'}\psi_{\beta}^{S}\left(\bar{\rho}^{'}\right)dl^{'}+\sum_{\alpha}\frac{c_{\beta\alpha}^{L}\psi_{\alpha}^{\Omega}\left(\bar{\rho}\right)}{\left(k_{\alpha}^{\Omega}\right)^2-\left(k_L^{\Omega}\right)^2}=0 \tag{9}$$

where

$$c_{\beta\alpha}^{L}=\frac{k^2-\left(k_L^{\Omega}\right)^2}{\left(k_{\alpha}^{\Omega}\right)^2-k^2}\int_{\sigma}\psi_{\alpha}^{\Omega}\left(\bar{\rho}^{'}\right)\hat{n}_{out}^{'}\cdot\bar{\nabla}_t^{'}\psi_{\beta}^{S}\left(\bar{\rho}^{'}\right)dl^{'} \tag{10}$$

The superscript L denotes low wavenumber.

Using pulse basis function and point matching in Eq. (9), we discretize the integral boundary σ into N segments. Let $z_{\beta n}$ be the surface unknown of the n_{th} patch.

$$z_{\beta n}=\left[\hat{n}_{out}^{'}\cdot\bar{\nabla}_t^{'}\psi_{\beta}^{S}\left(\bar{\rho}^{'}\right)\right]_{\bar{\rho}^{'}=\bar{\rho}_n^{\sigma}}\Delta t_n^{\sigma} \tag{11}$$

where $\bar{\rho}_n^{\sigma}$ is the center of the n_{th} segment on σ and Δt_n^{σ} is the length of the segment. Substituting Eq. (11) into Eq. (9) gives the matrix equation.

$$\overline{\overline{C}}^{L}\bar{z}_{\beta}+\overline{\overline{R}}^{L}\bar{c}_{\beta}^{L}=\bar{0} \tag{12}$$

where the matrix elements of $\overline{\overline{C}}^{L}$ and $\overline{\overline{R}}^{L}$ are given by, respectively,

$$C_{mn}^{L}=\frac{1}{\Delta t_n^{\sigma}}\int_{\sigma^{(n)}}g_E^{\Omega}\left(k_L^{\Omega},\bar{\rho}_m^{\sigma},\bar{\rho}^{'}\right)dl^{'} \tag{13}$$

$$R_{m\alpha}^{L}=\frac{\psi_{\alpha}^{\Omega}\left(\bar{\rho}_m^{\sigma}\right)}{\left(k_{\alpha}^{\Omega}\right)^2-\left(k_L^{\Omega}\right)^2} \tag{14}$$

In Eqs. (13) and (14), $\bar{\rho}_m^{\sigma}$ is the testing point on σ.

Similarly, we apply pulse basis function and point matching to the SIE in Eq. (10) to obtain the matrix equation.

$$\overline{\overline{D}}^{L}\bar{c}_{\beta}^{L}+\left[\overline{\overline{R}}^{L}\right]^{T}\bar{z}_{\beta}=\overline{\overline{E}}_{\beta}^{L}\bar{c}_{\beta}^{L} \tag{15}$$

where both $\overline{\overline{D}}^{L}$ and $\overline{\overline{E}}_{\beta}^{L}$ are diagonal matrices with matrix elements given by

$$E_{\beta}^{L}=\frac{1}{\left(k_{\beta}^{S}\right)^2-\left(k_L^{\Omega}\right)^2} \tag{16}$$

$$D_{\alpha}^{L}=\frac{1}{\left(k_{\alpha}^{\Omega}\right)^2-\left(k_L^{\Omega}\right)^2} \tag{17}$$

Substituting Eq. (12) into Eq. (15) gives the linear matrix equation that governs the eigenvalue problem,

$$\left[\overline{\overline{D}}^{L}-\left[\overline{\overline{R}}^{L}\right]^{T}\left(\overline{\overline{C}}^{L}\right)^{-1}\overline{\overline{R}}^{L}\right]\bar{c}_{\beta}^{L}=E_{\beta}^{L}\bar{c}_{\beta}^{L} \tag{18}$$

where the superscript T denotes the transpose of matrix. In Equation (18), vector $\bar{c}_{\beta}^{L}$ is the eigenvector and is E_{β}^{L} the corresponding eigenvalue. The resonant wavenumber k_{β}^{S} is calculated from the eigenvalue E_{β}^{L} using Eq. (16). Note that the matrix on the left hand side of Eq. (18) is independent of wavenumber so that the eigenvalues and eigenvectors are solved simultaneously. If the free space Green's function, instead of BBGFL, is used, the left hand side is a function of the wavenumber making the eigenvalue problem nonlinear. For nonlinear eigenvalue problem, an iterative search needs to be conducted for each eigenvalue. We rewrite Eq. (18) as

$$\overline{\overline{P}}^{L}\bar{c}_{\beta}^{L}=\lambda_{\beta}^{L}\bar{c}_{\beta}^{L} \tag{19}$$

where $\overline{\overline{P}}^{L}$ represents the matrix on the left-hand side of Eq. (18). The resonant wavenumbers are calculated from the eigenvalues λ_β^L.

$$k_\beta^S = \sqrt{\left(k_L^\Omega\right)^2 + \frac{1}{\lambda_\beta^L}} \tag{20}$$

2.2. Normalization of Modal Function of S Waveguide

After solving $\bar{c}_\beta^L$, we use Eq. (8) to compute the unnormalized modal functions ψ_β^S. It can be shown that modes are orthogonal. Since the Green's functions are expressed in terms of normalized modes, we next normalize the modes. The normalization of modal function is the condition

$$\iint_S \left(\psi_\beta^S\left(\bar{\rho}\right)\right)^2 dxdy = 1 \tag{21}$$

From (4) and (8), we have,

$$\sum_{n=1}^{N} z_{\beta n} \frac{1}{\Delta t_n^\sigma} \int_\sigma^{(n)} g_E^\Omega\left(k_L^\Omega, \bar{\rho}, \bar{\rho}^{'}\right) dll' + \sum_\alpha \frac{c_{\beta\alpha}^L \psi_\alpha^\Omega\left(\bar{\rho}\right)}{\left(k_\alpha^\Omega\right)^2 - \left(k_L^\Omega\right)^2} = \begin{cases} \psi_\beta^S\left(\bar{\rho}\right) & \text{for } \bar{\rho} \text{ inside } S \\ 0 & \text{for } \bar{\rho} \text{ outside } S \end{cases} \tag{22}$$

Take the Laplacian on both sides of Eq. (21) and apply the low wavenumber conditions, $k_L^\Omega \ll k_\alpha^\Omega$ and $k_L^\Omega \ll k_\beta^S$, Equation (21) can be approximated as

$$\frac{1}{\left(k_\beta^S\right)^2} \sum_\alpha c_{\beta\alpha}^L \psi_\alpha^\Omega\left(\bar{\rho}\right) \cong \begin{cases} \psi_\beta^S\left(\bar{\rho}\right) & \text{for } \bar{\rho} \text{ inside } S \\ 0 & \text{for } \bar{\rho} \text{ outside } S \end{cases} \tag{23}$$

Using Eq. (23), we then have

$$\iint_{\Omega - S} \left[\frac{1}{\left(k_\beta^S\right)^2} \sum_\alpha c_{\beta\alpha}^L \psi_\alpha^\Omega\left(\bar{\rho}\right)\right]^2 dxdy = 0 \tag{24}$$

The normalization condition of Eq. (21) becomes

$$\iint_\Omega \left[\frac{1}{\left(k_\beta^S\right)^2} \sum_\alpha c_{\beta\alpha}^L \psi_\alpha^\Omega\left(\bar{\rho}\right)\right]^2 dxdy = 1 \tag{25}$$

This leads to the normalization condition for the modal function ψ_β^S

$$\frac{1}{\left(k_\beta^S\right)^4} \sum_\alpha \left(c_{\beta\alpha}^L\right)^2 = 1 \tag{26}$$

Hence, the normalized modal function ψ_β^S of the S waveguide is expressed in terms of the modal functions ψ_α^Ω of rectangular waveguide as follows

$$\psi_\beta^S\left(\bar{\rho}\right) = \frac{1}{\sqrt{\sum_\alpha \left(\tilde{c}_{\beta\alpha}^L\right)^2}} \sum_\alpha \tilde{c}_{\beta\alpha}^L \psi_\alpha^\Omega\left(\bar{\rho}\right) \tag{27}$$

where we have used the symbol $\sim$ to represent the un-normalized eigenvectors $\tilde{\bar{c}}_\beta^L$. We now use the resonant wavenumbers k_β^S in Eq. (20) and the normalized modal function $\psi_\beta^S(\bar{\rho})$ in Eq. (27) to construct the modal representation of Green's function g_E^S for the waveguide S in Eq. (5).

2.3. Higher Order Convergence for S Waveguide

For the S waveguide, we next derive a higher order extraction BBGFL for $g_E^S(k,\bar{\rho},\bar{\rho}^{'})$ with a convergence of $1/(k_\beta^S)^6$.

With a low wavenumber extraction at k_L^S, the Green's function g_E^S can be expressed as

$$g_E^S\left(\omega,\bar{\rho},\bar{\rho}^{'}\right)=g_E^S\left(\omega_L^S,\bar{\rho},\bar{\rho}^{'}\right)+\sum_\beta\frac{\omega-\omega_L^S}{\left[\left(k_\beta^S\right)^2-\omega\right]\left[\left(k_\beta^S\right)^2-\omega_L^S\right]}\psi_\beta^S\left(\bar{\rho}\right)\psi_\beta^S\left(\bar{\rho}'\right) \tag{28}$$

where $\omega=k^2$ and $\omega_L^S=(k_L^S)^2$. Next, we take the difference of g_E^S at two additional low wavenumbers: $\omega=\omega_L^S+\frac{\Delta\omega_L^S}{2}$ and $\omega=\omega_L^S-\frac{\Delta\omega_L^S}{2}$. Then

$$\begin{aligned}&g_E^S\left(\omega_L^S+\frac{\Delta\omega_L^S}{2},\bar{\rho},\bar{\rho}^{'}\right)-g_E^S\left(\omega_L^S-\frac{\Delta\omega_L^S}{2},\bar{\rho},\bar{\rho}^{'}\right)\\&=\sum_\beta\frac{\Delta\omega_L^S}{\left[\left(k_\beta^S\right)^2-\left(\omega_L^S+\frac{\Delta\omega_L^S}{2}\right)\right]\left[\left(k_\beta^S\right)^2-\left(\omega_L^S-\frac{\Delta\omega_L^S}{2}\right)\right]}\psi_\beta^S\left(\bar{\rho}\right)\psi_\beta^S\left(\bar{\rho}'\right)\end{aligned} \tag{29}$$

Using Equation (29), Equation (28) becomes

$$\begin{aligned}g_E^S\left(\omega,\bar{\rho},\bar{\rho}^{'}\right)\;=\;&g_E^S\left(\omega_L^S,\bar{\rho},\bar{\rho}^{'}\right)+\frac{\omega-\omega_L^S}{\Delta\omega_L^S}\left[g_E^S\left(\omega_L^S+\frac{\Delta\omega_L^S}{2},\bar{\rho},\bar{\rho}^{'}\right)-g_E^S\left(\omega_L^S-\frac{\Delta\omega_L^S}{2},\bar{\rho},\bar{\rho}^{'}\right)\right]\\&+\sum_\beta\frac{\left(\omega-\omega_L^S\right)^2\psi_\beta^S\left(\bar{\rho}\right)\psi_\beta^S\left(\bar{\rho}'\right)}{\left[\left(k_\beta^S\right)^2-\omega\right]\left[\left(k_\beta^S\right)^2-\omega_L^S-\frac{\Delta\omega_L^S}{2}\right]\left[\left(k_\beta^S\right)^2-\omega_L^S+\frac{\Delta\omega_L^S}{2}\right]}\\&-\sum_\beta\frac{\left(\omega-\omega_L^S\right)\left(\frac{\Delta\omega_L^S}{2}\right)^2\psi_\beta^S\left(\bar{\rho}\right)\psi_\beta^S\left(\bar{\rho}'\right)}{\left[\left(k_\beta^S\right)^2-\omega\right]\left[\left(k_\beta^S\right)^2-\omega_L\right]\left[\left(k_\beta^S\right)^2-\omega_L^S-\frac{\Delta\omega_L^S}{2}\right]\left[\left(k_\beta^S\right)^2-\omega_L^S+\frac{\Delta\omega_L^S}{2}\right]}\end{aligned} \tag{30}$$

The expression (30) consists of three low wavenumber extractions at $\omega=\omega_L^S$, $\omega=\omega_L^S+\frac{\Delta\omega_L^S}{2}$ and $\omega=\omega_L^S-\frac{\Delta\omega_L^S}{2}$. It is clear in Eq. (30) that the modal summation over β converges as $1/(k_\beta^S)^6$ giving a higher order extraction Green's function g_E^S with an accelerated convergence.

Table 1. First 20 resonant wavenumber of waveguide S.

β	k_β^S (MoM) $[m^{-1}]$	k_β^S (BBGFL) $[m^{-1}]$	k_β^S (HFSS) $[m^{-1}]$		β	k_β^S (MoM) $[m^{-1}]$	k_β^S (BBGFL) $[m^{-1}]$	k_β^S (HFSS) $[m^{-1}]$
1	383.2	383.2	374.9		11	1112.4	1112.8	1092.6
2	563.3	563.3	557.1		12	1176.2	1176.6	1169.1
3	627.5	627.5	611.2		13	1241.5	1241.9	1240.6
4	741.2	741.2	740.3		14	1268.5	1268.9	1268.0
5	800.3	800.3	796.8		15	1283.0	1283.4	1283.0
6	860.1	860.1	843.4		16	1371.4	1371.8	NA
7	943.3	943.7	918.7		17	1382.6	1383.9	NA
8	992.4	992.8	994.6		18	1445.4	1446.7	NA
9	1030.9	1030.5	1032.3		19	1505.8	1506.7	NA
10	1086.5	1086.5	1071.6		20	1523.8	1525.6	NA

3. NUMERICAL RESULTS

We use the higher order BBGFL method to calculate the broadband Green's function for the S waveguide shown in Figure 1(c). The dimensions of waveguide S are $L_x = 500$ mils, $L_y = 500$ mils, $W_x = 100$ mils, and $W_y = 250$ mils.

Table 1 lists the first 20 resonant wavenumbers computed by using BBGFL. These are compared with the results from MoM and HFSS for the waveguide S. The relative permittivity is lossless with $\varepsilon_r = 4.4$. For HFSS, we only calculate the first 15 resonant modes because of the much larger CPU required for larger resonant wavenumbers. The results are in excellent agreement among BBGFL, MoM and HFSS. The corresponding 20 normalized modal functions computed using BBGFL are plotted in Figure 2. The modal functions are displayed within the waveguide S. The figure shows that the structures of modal functions become more complicated for larger k_β^S. The figure also shows that the modal distributions calculated by HFSS agree with BBGFL.

Note that evanescent modes are required for convergence. Evanescent modes are modes with higher resonant wavenumbers than the maximum operating wavenumber of interest. For example, if the maximum interested frequency is 20 GHz, then the broadband Green's functions will cover six

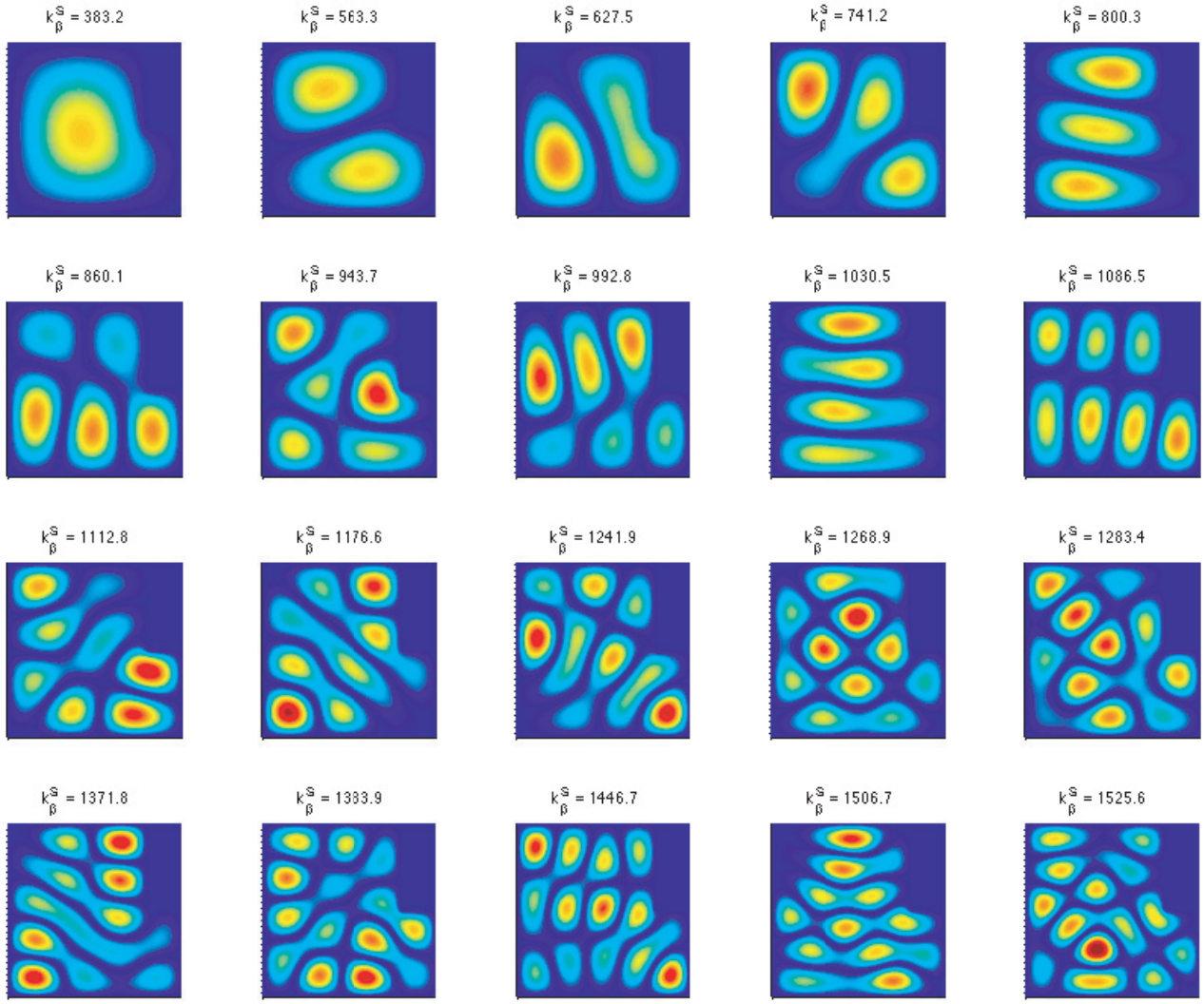

Figure 2. Modal functions of the first 20 resonant modes of waveguide S. All plots are in the same scale, $x = -250$ mils ~ 250 mils and $y = -250$ mils ~ 250 mils.

Table 2. List of 6 wavenumbers and the number of resonant modes for $f_{\max} = 20\,\text{GHz}$.

	$k_{\max}$	$1.1k_{\max}$	$1.2k_{\max}$	$1.3k_{\max}$	$1.5k_{\max}$	$2k_{\max}$
wavenumber	880	968	1056	1144	1320	1760
number of k_β^S	6	7	9	11	15	27

resonant modes at 8.71 GHz, 12.81 GHz, 14.27 GHz, 16.86 GHz, 18.2 GHz, and 19.56 GHz. Thus for $f_{\max}$ at 20 GHz, the corresponding maximum operating wavenumber $k_{\max}$ is 880. The modal expansion needs to have resonant wavenumbers larger $k_{\max}$ to attain a convergent summation. How much larger depends on the rate of convergence. In Table 2, we list the number of resonant modes which will be included in the summation versus the multiples of $k_{\max}$, covered in the spectrum.

We next compare the convergence for the Green's functions of waveguide S computed using 3 different methods: the direct modal summation of Eq. (5) with a 2nd order convergence,the single low wavenumber extraction BBGFL of Eq. (28) with a 4th order convergence, and the three low wavenumber extraction BBGFL of Eq. (30) with a 6th order convergence. The comparison is based on the number of resonant modes required in the summation. The direct MoM solutionis used as a reference for comparison. In the following, we consider three cases.

Case I: lossless waveguide with $\varepsilon_r = 4.4$. The source point is at $x = 30\,\text{mils}$ and $y = 20\,\text{mils}$. The observation points are at $x = -250\,\text{mils}$ to 250 mils and $y = -50\,\text{mils}$.

Since the dielectric is lossless, the Green's function is purely real. In Figure 3, we compare the Green's function at 20 GHz computed by the three different modal solutions and MoM.The numbers of modes are varied from 6 to 27. As we include more modes, we see that the results of modal summation are in better agreement with MoM. Compared to the 4th order BBGFL, the 6th order BBGFL requires less number of modes (11 modes) to converge to MoM. The direct modal summation (2nd order) is not in good agreement with MoM even with 27 modes in the summation.

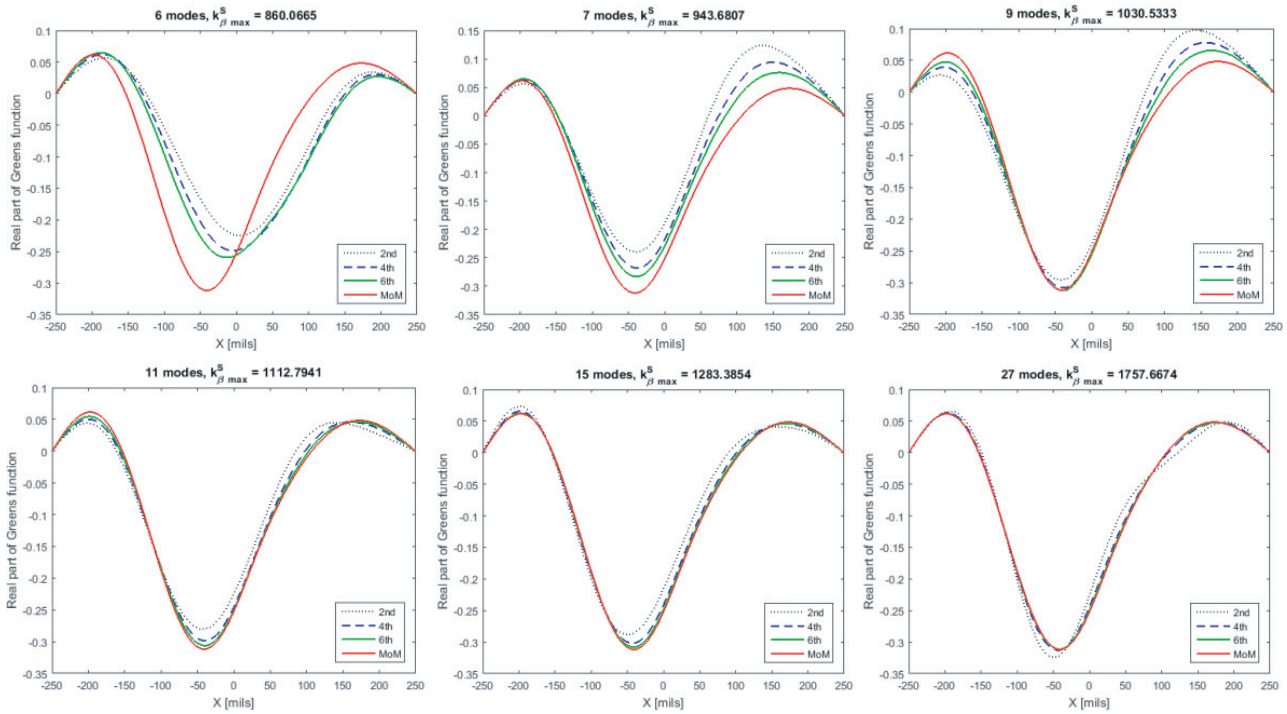

Figure 3. Case I with the observation point at $x = -250\,\text{mils} \sim 250\,\text{mils}$ and $y = -50\,\text{mils}$. The real parts of Green's functions are shown for the 2nd, 4th, 6th order, and MoM at 20 GHz. The number of mode accumulations are 6, 7, 9, 11, 15, and 27.

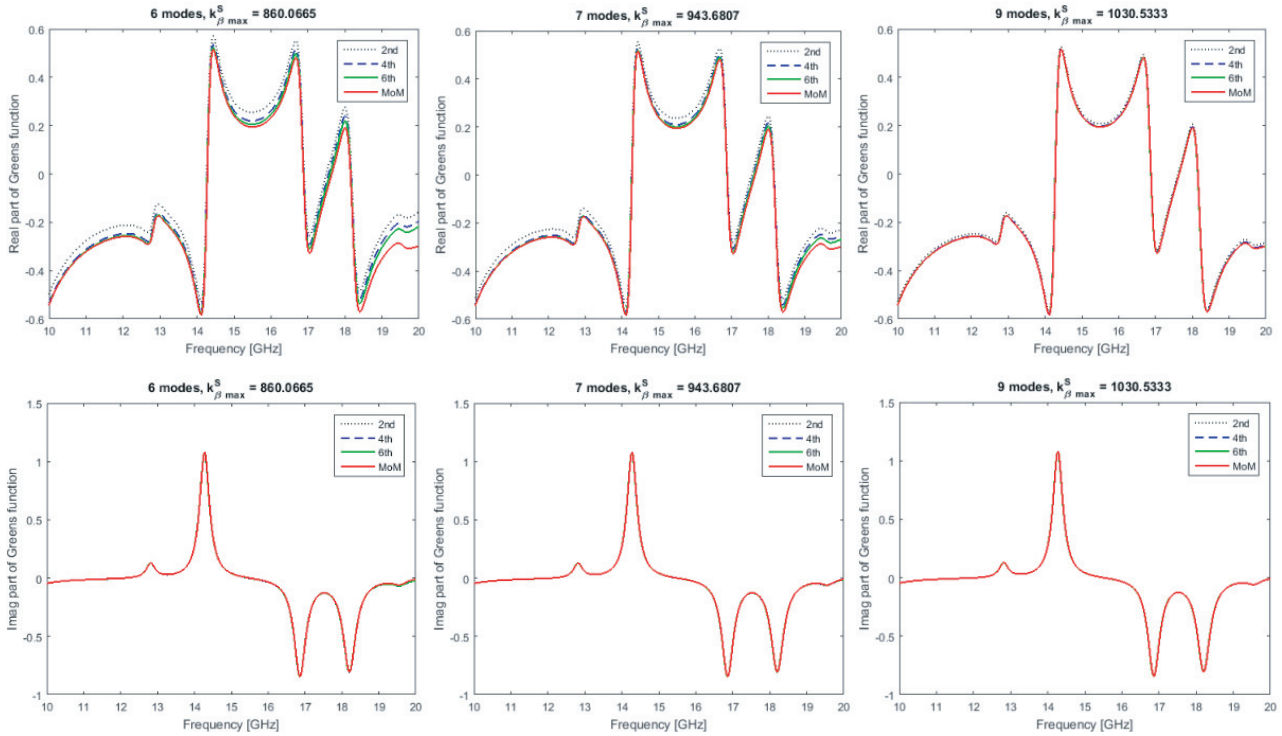

Figure 4. Case II with the observation point at $x = -50$ mils and $y = -50$ mils. First row shows the real parts of Green's function for the 2nd, 4th, 6th order approaches, and MoM over the frequency range of 10 GHz to 20 GHz. The number of mode accumulations are 6, 7, and 9. The second row shows the comparison of corresponding imaginary parts of the Green's function frequency responses.

Next, we consider lossy dielectric cases with a small loss tangent. We compare the frequency responses of, the Green's functions, and the mean errors from the three modal summation methods using MoM solution as the reference.

Case II: lossy waveguide with $\varepsilon_r = 4.4(1 - j0.023)$. The source point is at $x = 30$,mils and $y = 20$ mils. The observation points are at $x = -250$ mils to 250 mils and $y = -50$ mils.

In this case, the source is not close to the observation. In Figure 4, the comparisons are made on the real and imaginary parts of Green's function over frequencies from 10 to 20 GHz at the observation point $x = -50$ mils and $y = -50$ mils. We observe 5 resonances at the frequencies: 12.81 GHz, 14.27 GHz, and 16.86 GHz, 18.2 GHz, and 19.56 GHz. As we increase the modal expansion from 6 to 9 modes, the real parts are in better agreement with the MoM results. We notice that the results of the 6th order BBGFL are in better agreement with MoM than the results of the other two modal summation. However, the comparisons of imaginary parts do not show significant differences among these 4 methods. Thereafter, we will only compare the real parts of the Green's functions.

In Figure 5, we compare the real part of Green's function at the resonant frequency 19.56 GHz. The number of modes in the modal expansion varies from 6 to 27. Since the source is not close to the observation, the spatial response of Green's function varies smoothly. Similar to the case I in Figure 3, the 6th order BBGFL requires 11 modes to converge which is smaller than those required of the 4th order BBGFL and the direct modal summation (2nd order) approach.

Case III: lossy waveguide with $\varepsilon_r = 4.4(1 - j0.023)$. The source point is at $x = 30$ mils and $y = -50$ mils. The observation points are at $x = -250$ mils to 250 mils and $y = -50$ mils.

In this case, the line of observation points include the source point. The spatial responses of Green's function are expected to have more variations. Figure 6 shows the frequency response for the real parts of Green's functions with different number of modes included in the modal summations. We also observe five resonances between 10 and 20 GHz. Compared to Figure 4, Case III requires more modes to converge. The 6th order BBGFL still converges fastest as only 9 modes are needed, while the

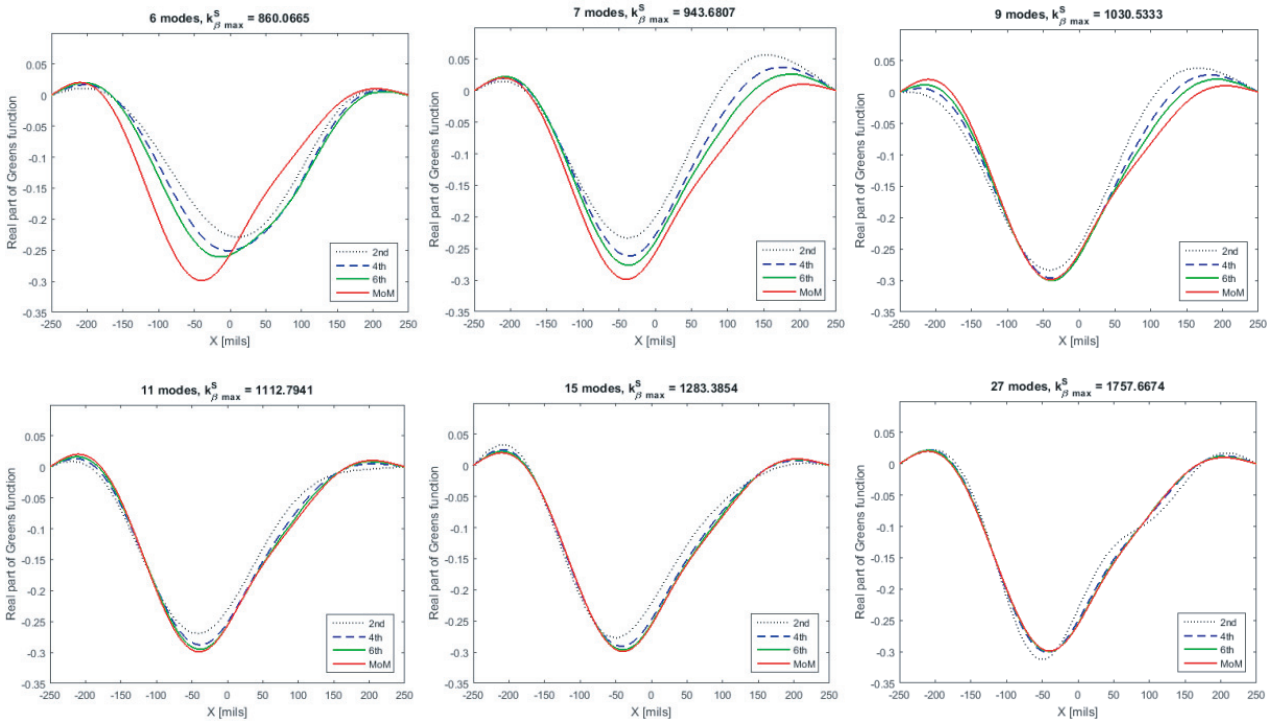

Figure 5. Case II with the observation point at $x = -250$ mils ~ 250 mils and $y = -50$ mils. The real parts of Green's functions are shown for the 2nd, 4th, 6th order, and MoM at 19.56 GHz. The number of mode accumulations are 6, 7, 9, 11, 15, and 27.

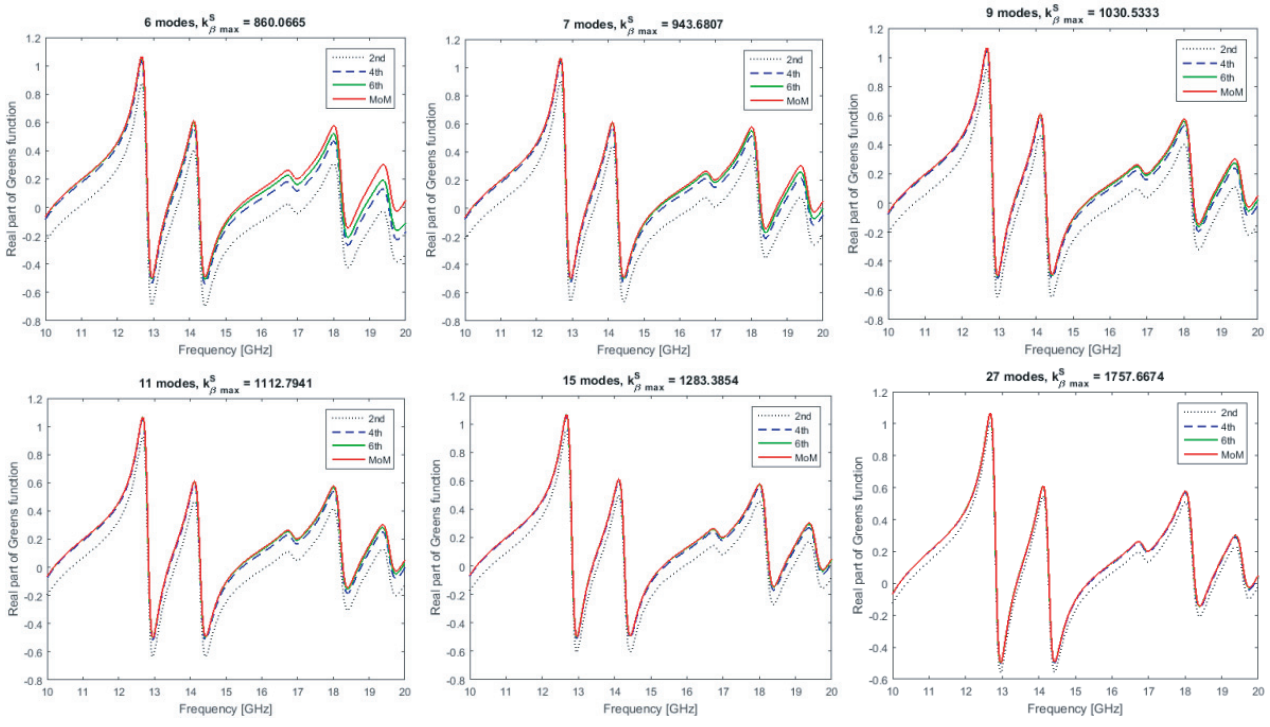

Figure 6. Case III with the source point at $x = 50$ mils and $y = -50$ mils. The real parts of Green's functions are shown for the 2nd, 4th, 6th order, and MoM over 10 GHz to 20 GHz. The number of mode accumulations are 6, 7, 9, 11, 15, and 27.

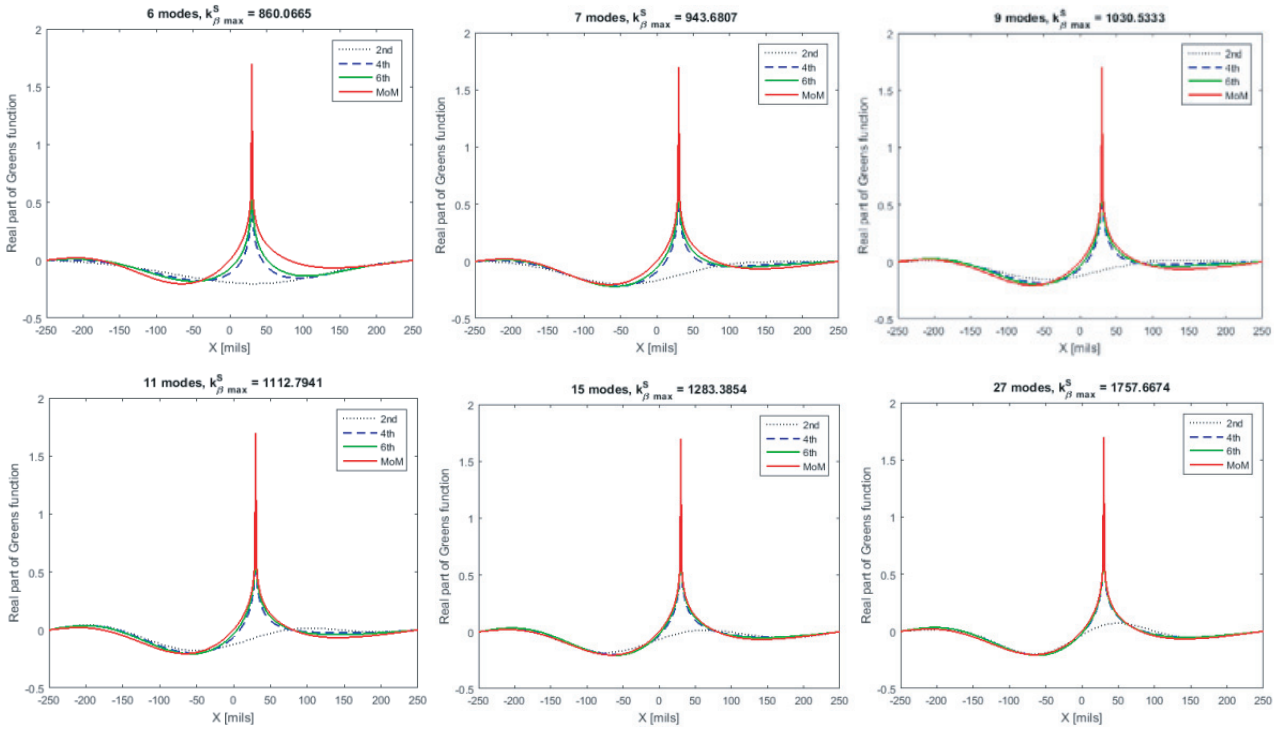

Figure 7. Case III with the observation at $x = -250$ mils ~ 250 mils and $y = -50$ mils. The real parts of Green's functions are shown for the 2nd, 4th, 6th order, and MoM at 19.56 GHz. The number of mode accumulations are 6, 7, 9, 11, 15, and 27.

4th order BBGFL requires 15 modes to agree with MoM. The spatial responses of Green's functions at the resonant frequency 19.56 GHz are plotted in Figure 7. A sharp peak is observed at $x = 30$ mils where the Green's function becomes singular. In this case, because of the resonance and close to the singular point, the modal expansion requires more modes for convergence. Nevertheless, the 6th order BBGFL still requires less number of modes to agree with MoM. We note that the 2nd order expansion cannot exhibit the singular behavior of Green's function even with 27 modes. This confirms the advantage of low wavenumber extraction to accelerate the convergence of modal summation.

In Figures 8 and 9, we compare the mean errors between the direct modal summation (2nd order), 4th order BBGFL, and 6th order BBGFL for lossy dielectric cases II and III. The MoM results are used as the reference. The observation points are at $x = -250$ mils to 250 mils and $y = -50$ mils. We use 2000 frequency points from 0 to 20 GHz. Both cases show that the 6th order BBGFL converges faster than the 4th order BBGFL and much faster than the 2nd order modal expansion. For case II, it takes 9 modes for the 6th order BBGFL to achieve the error less than 1%. The faster convergence of 6th order BBGFL becomes more apparent in case III where the observation points include the source point. To achieve less than 1% error, the 6th order BBGFL requires 9 modes while the 4th order BBGFL requires 21 modes. In case III, the 2nd order approach cannot lower the mean error to less than 10% even with 80 mode accumulations. This shows that the higher order extraction of BBGFL developed can maintain faster convergence even when the Green's function is close to the singularity.

To calculate the S waveguide modes, we have used 961 rectangular waveguide modes in the Equation (19) of the linear eigenvalue problem. This means the resonant wavenumber k^{Ω}_{α} of the rectangular waveguide with $\alpha = 1, 2, \ldots, 961$. This number is more than sufficient as our purpose is to demonstrate the accuracies for the construction of S waveguide modes. In terms of the number of resonant wavenumbers, the 6th order BBGFL only needs to cover resonant wavenumbers up to $1.2k_{\max}$ for both cases II and III, while the 4th order BBGFL require more modes from up to $2k_{\max}$. Moreover, for case III, the 6th order BBGFL requires less than half the number of modes needed for the 4th order BBGFL. It is evident that both 6th and 4th order BBGFL outperform the direct modal summation

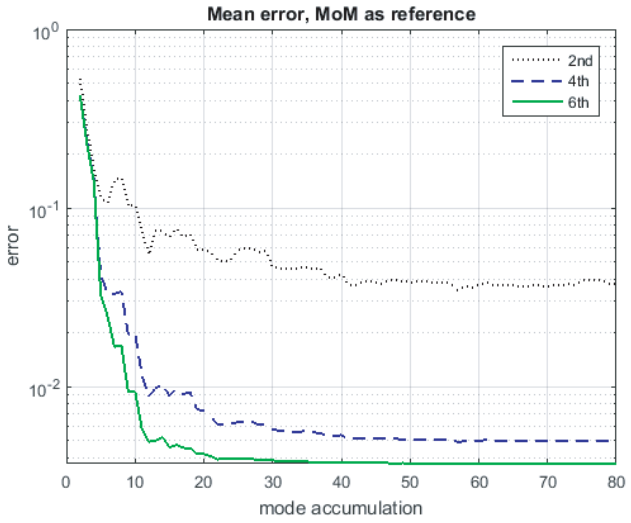

Figure 8. Mean errors for the 2nd, 4th, and 6th order using MoM as reference for the case II.

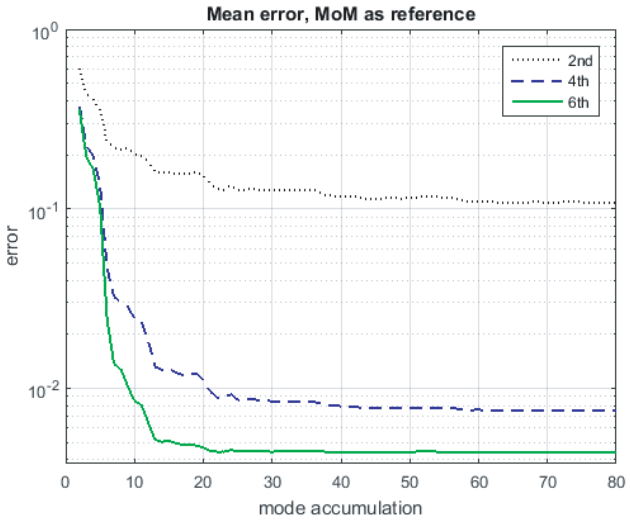

Figure 9. Mean errors for the 2nd, 4th, and 6th order using MoM as reference for the case III.

approach (2nd order).

In Table 3, we show the CPU time for BBGFL and MoM for the simulations of case III. The computations were performed using Intel i5-4690@3.5 GHz with 8 GB memory. For the higher order extraction, the computations consist of three parts: finding the modes through linear eigenvalue problem of BBGFL, three low wavenumber extractions calculations for the S waveguide, and the broadband computation. For the 6th order BBGFL, the total CPU time is 8.6 seconds for computing 2000 frequency Green's function responses. For the MoM, it requires 2000 computations with the same computation complexities for each frequency response. The total CPU time for MoM is 675.8 seconds which is much larger than the BBGFL.

Table 3. CPU time comparison between High order extraction of BBGFL with MoM.

	High order extraction (6th order)	MoM
Preset (Find all modes)	2.4 sec	$2000 * 0.3379 =$ **675.8 sec**
Low wavenumbers extraction	0.51 sec	
Broadband computation	$2000 * 0.00285 = 5.7$ sec	
Total Time	**8.6 sec**	

4. CONCLUSION

In this paper, we develop a higher order extraction (6th order) BBGFL method to efficiently compute the broadband frequency responses of Green's functions. The approach combines the modal expansion representation of Green's function with three low wavenumber extractions. The higher order method shows that the modal summation converges at the rate of $1/(k_\beta^S)^6$ which is a faster convergence than the BI-RME and BBGFL methods both with $1/(k_\beta^S)^4$ convergence. The higher order extraction BBGFL demonstrates that a less number of evanescent modes are required in modal summation for the broadband Green's function. This also means that less number of rectangular waveguide modes are required to construct the modal functions of the S waveguide. The 6th order extraction BBGFL requires a similar computation time as the 4th order BBGFL but with a faster convergence. The BBGFL is useful and has been used in formulating integral equations for more complex problems [11, 12].

The proposed technique best uses the existing knowledge of Green's functions of regular geometry to fast compute Green's functions of arbitrary shaped waveguide. The higher order extraction technique further accelerates the convergence of broadband Green's functions. This paper demonstrates waveguide with TM polarization. The acceleration scheme can also be applied to BBGFL for TE polarization which will be a subject of future study. Previously the TE problem has been solved with BBGFL using a single low wavenumber extraction [11–13].

APPENDIX A.

There are two parts of BBGFL that require the calculations using MoM. The first part is to calculate the rectangular waveguide Green's function at low wavenumber k_L^Ω on the boundary σ. We write g_E^Ω as a sum of free space Green's function g_0 and the response g_{ER}^Ω in Ω.

$$g_E^\Omega\left(k,\bar{\rho},\bar{\rho}^{'}\right) = g_0\left(k,\bar{\rho},\bar{\rho}^{'}\right) + g_{ER}^\Omega\left(k,\bar{\rho},\bar{\rho}^{'}\right) \tag{A1}$$

In Equation (13), we have to compute the matrix elements for the non-self and self-patch integrals. The respective expressions are shown in (A2) and (A3).

$$C_{mn}^L = g_0\left(k_L^\Omega,\bar{\rho}_m^\sigma,\bar{\rho}_n^\sigma\right) + g_{ER}^\Omega\left(k_L^\Omega,\bar{\rho}_m^\sigma,\bar{\rho}_n^\sigma\right) \quad \text{for } m \neq n \tag{A2}$$

$$C_{mm}^L = \frac{1}{4j}\left(1 - \frac{2j}{\pi} ln\left(\frac{\gamma k_L}{4e}\Delta t_m^\sigma\right)\right) + g_{ER}^\Omega\left(k_L^\Omega,\bar{\rho}_m^\sigma,\bar{\rho}_n^\sigma\right) \tag{A3}$$

where $\gamma = 1.78107$ is the Euler constant. The response Green's function g_{ER}^Ω can be computed using MoM.

The second part requiring MoM is the low wavenumber extraction for waveguide S. We write g_E^S as a sum free space Green's function and the response in S.

$$g_E^S\left(k,\bar{\rho},\bar{\rho}^{''}\right) = g_0\left(k,\bar{\rho},\bar{\rho}^{''}\right) + g_{ER}^S\left(k,\bar{\rho},\bar{\rho}^{''}\right) \tag{A4}$$

The response Green's function g_{ER}^S is calculated by solving the SIE in Eq. (A5). The filling of impedance matrix is similar to the first term on the right hand sides of Eqs. (A2) and (A3). After solving the surface unknowns, the response g_{ER}^S can be found using Eq. (A6) below. Note that, MoM calculations have to be performed separately for each of the 3 low wavenumbers.

$$\int_{\partial S} g_0\left(k,\bar{\rho},\bar{\rho}^{'}\right)\hat{n}_{out}^{'}\cdot\nabla_t^{'} g_E^S\left(k,\bar{\rho}^{'},\bar{\rho}^{''}\right)dl^{'} = -g_0\left(k,\bar{\rho},\bar{\rho}^{''}\right) \tag{A5}$$

$$g_{ER}^S\left(k,\bar{\rho},\bar{\rho}^{''}\right) = \int_{\partial S} g_0\left(k,\bar{\rho},\bar{\rho}^{'}\right)\hat{n}_{out}^{'}\cdot\nabla_t^{'} g_E^S\left(k,\bar{\rho}^{'},\bar{\rho}^{''}\right)dl^{'} \tag{A6}$$

REFERENCES

1. Tai, C. T., *Dyadic Green Functions in Electromagnetic Theory*, IEEE Press, 1994.
2. Collin, R. E., *Field Theory of Guided Waves*, IEEE Press, 1991.
3. Felsen, L. B. and N. Marcuvitz, *Radiation and Scattering of Waves*, Wiley, 1994.
4. Harrington, R. F. and J. L. Harrington, *Field Computation by Moment Methods*, Oxford University Press, Oxford, UK, 1996.
5. Tsang, L., H. Chen, C. C. Huang, and V. Jandhyala, "Modeling of multiple scattering among vias in planar waveguides using Foldy-Lax equations," *Microw. Opt. Tech. Lett.*, Vol. 31, 201–208, Nov. 2001.
6. Chen, H., Q. Li, L. Tsang, C. C. Huang, and V. Jandhyala, "Analysis of large number of vias and differential signaling in multi-layered structures," *IEEE Trans. on Microw. Theory and Tech.*, Vol. 51, 818–829, Mar. 2003.

7. Chang, X. and L. Tsang, "Fast and broadband modeling method for multiple vias with irregular antipad in arbitrarily shaped power/ground planes in 3-D IC and packaging based on generalized Foldy-Lax equations," *IEEE Trans. Compon. Packag. Manuf. Technol.*, Vol. 4, No. 4, 685–696, Apr. 2014.
8. Conciauro, G., M. Guglielmi, and R. Sorrentino, *Advanced Modal Analysis: CAD Techniques for Waveguide Components and Filters*, Wiley, NY, USA, 2002.
9. Bozzi, M., L. Perregrini, and K. Wu, "Modeling of conductor, dielectric, and radiation losses in substrate integrated waveguide by the boundary integral-resonant mode expansion method," *IEEE Trans. Microw. Theory Tech.*, Vol. 56, No. 12, 3153–3161, Dec. 2008.
10. Arcioni, P., M. Bozzi, M. Bressan, G. Conciauro, and L. Perregrini, "The BI-RME method: An historical overview," *2014 International Conference on Numerical Electromagnetic Modeling and Optimization for RF, Microwave, and Terahertz Applications (NEMO)*, May 14–16, 2014.
11. Tsang, L. and S. Huang, "Full wave modeling and simulations of the waveguide behavior of printed circuit boards using a broadband Green's function technique," Provisional U.S. Patent No. 62/152.702, Apr. 24, 2015.
12. Huang, S., "Broadband Green's function and applications to fast electromagnetic analysis of high-speed interconnects," Ph.D. dissertation, Dept. Elect. Eng., Univ. Washington, Seattle, WA, Jun. 2015.
13. Tsang, L. and S. Huang, "Broadband Green's function with low wavenumber extraction for arbitrary shaped waveguide and applications to modeling of vias in finite power/ground plane," *Progress In Electromagnetic Research*, Vol. 152, 105–125, 2015.
14. Huang, S. and L. Tsang, "Fast electromagnetic analysis of emissions from printed circuit board using broadband Green's function method," *IEEE Trans. on Electromagnetic Compatibility*, Vol. 58, 1642–1652, 2016.
15. Tsang, L., "Broadband calculations of band diagrams in periodic structures using the broadband Green's function with low wavenumber extraction (BBGFL)," *Progress In Electromagnetics Research*, Vol. 153, 57–68, 2015.
16. Tsang, L. and S. Tan, "Calculations of band diagrams and low frequency dispersion relations of 2D periodic dielectric scattering using broadband Green's function with low wavenumber extraction (BBGFL)," *Optics Express*, Vol. 24, No. 2, 945–965, 2016.